Performance enhancement of a phase-change-material based thermal energy storage device for air-conditioning applications

Nie, Binjian; Du, Zheng; Zou, Boyang; Li, Yongliang; Ding, Yulong

DOI:
10.1016/j.enbuild.2020.109895

Document Version
Peer reviewed version

Citation for published version (Harvard):
Nie, B, Du, Z, Zou, B, Li, Y & Ding, Y 2020, 'Performance enhancement of a phase-change-material based thermal energy storage device for air-conditioning applications', *Energy and Buildings*, vol. 214, 109895, pp. 1-12. https://doi.org/10.1016/j.enbuild.2020.109895

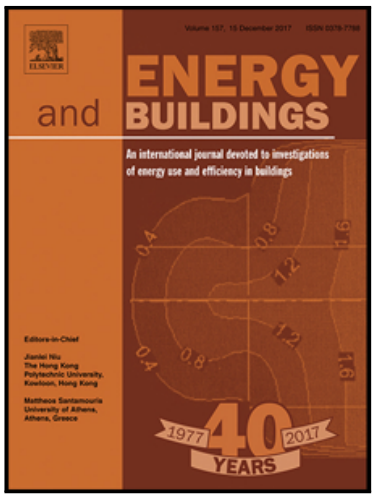

Performance enhancement of a phase-change-material based thermal energy storage device for air-conditioning applications

Binjian Nie , Zheng Du , Boyang Zou , Yongliang Li , Yulong Ding

PII: S0378-7788(19)32594-0
DOI: https://doi.org/10.1016/j.enbuild.2020.109895
Reference: ENB 109895

To appear in: *Energy & Buildings*

Received date: 22 August 2019
Revised date: 21 November 2019
Accepted date: 21 February 2020

Please cite this article as: Binjian Nie , Zheng Du , Boyang Zou , Yongliang Li , Yulong Ding , Performance enhancement of a phase-change-material based thermal energy storage device for air-conditioning applications, *Energy & Buildings* (2020), doi: https://doi.org/10.1016/j.enbuild.2020.109895

HIGHLIGHTS

- Devices of four different configurations were modelled and compared;
- The air side fins are more effective than the PCM side fins;
- Adding fins and thermal conductivity improvement of PCM is comparable;
- An improved thermal comfort and reduced outlet temperature fluctuations was obtained.

Performance enhancement of a phase-change-material based thermal energy storage device for air-conditioning applications

Binjian Nie[a], Zheng Du[a,b], Boyang Zou[a], Yongliang Li[a], Yulong Ding[a]*

a. Birmingham Centre for Energy Storage, School of Chemical Engineering, University of Birmingham, Edgbaston, Birmingham B15 2TT, UK

b. Department of Materials Science and Engineering & Shenzhen Key Laboratory of Full

Spectral Solar Electricity Generation, Southern University of Science and Technology, Guangdong, 518055, China.

Email: Y.Ding@bham.ac.uk

Abstract

This work concerns performance enhancement of phase change material (PCM) based thermal energy storage (TES) devices for air-conditioning applications. Such devices have numerous potential applications in the building environment. The TES device often uses air as the heat transfer fluid and, as a result, its performance is often limited by heat transfer in either or both of the PCM and the air sides. This paper aims to overcome the heat transfer limitations through intensifying heat transfer using two methods of extending heat transfer surfaces (fins) in both the PCM and air sides and adding heat transfer enhancement materials in the PCM. First, a TES device with different configurations (no fins; offset strip fins on the air side only; straight fins on the PCM side only; offset strip fins on air side and straight fins on PCM side) and PCM with different thermal conductivities were modelled and compared. The comparison leads to an advantageous utilization of fins instead of adding thermal conductive particles. The results also indicated a significant extent of performance enhancement of the TES device due to the use of fins with the charging and discharging times reduced respectively by ~85% and ~74%. The airside fins were found to be more effective than the PCM side fins. The results also showed that the heat transfer enhancement due to the PCM side fins could be achieved by increasing PCM thermal conductivity. The modelling results were then validated by experimental data. Finally, a PCM-based TES device was

designed and manufactured based on the above results. The device was integrated into an air-conditioning system and experimentally tested. The results showed that, for both charge and discharge processes, the stabilization of the outlet temperature of the air conditioning system was significantly improved, leading to an increased extent of thermal comfort and decreased outlet temperature fluctuations. The obtained results can be used as the design guideline of the compact TES device for air conditioning.

Keywords: Thermal energy storage device, Phase change material, Air conditioning

Nomenclature

c_p Specific heat of capacity (kJ/(kg·K))

k Thermal conductivity (W/(m·K))

m Mass(kg)

$\dot{m}$ Mass flow rate (kg/s)

T Temperature (°C or K)

t Time (s)

RH Relative Humidity

H Latent heat (kJ/kg)

V Velocity vector (m/s)

ρ Density(kg/m^3)

h Specific enthalpy (kJ/kg)

λ Liquid fraction

p Pressure(Pa)

?? Liquid viscosity (Pa·s)

δ *Error*

y_{exp} *Experimental value*

y_{num} *Numerical value*

ΔR *total error*

δX_n *error factor*

Subscripts

l Liquid

s Solid

e End

m Melting

i Initial

Al Aluminium

ref Reference

max Maximum

ave Average

exp Experimental

num Numerical

1. Introduction

Energy-related issues such as global warming and environmental pollution have been a rising concern over the last few decades. The buildings sector contributes a significant portion to such issues due to the use of air-conditioning for generating thermal comfort [1]. Air-conditioning systems are typically designed to meet the peak demand, which is considerably higher than the average demand. This implies that air-conditioning systems are over-sized in terms of the average load and are often run at sub-optimal conditions[2]. In addition, standalone air-conditioning units often operate at a high stop-start frequently for temperature regulation, leading to more energy consumption, a higher level of noise and a shorter life-span[3]. This work aims to address these issues by using thermal energy storage with phase change materials (PCMs), which can significantly reduce the difference between the rated capacity and average capacity of air-conditioning systems and start-stop frequency, leading to lower power consumption and better consumer experience due to reduced noise. The reduction in the rated capacity of air-conditioning systems also means a reduced weight, which is the primary motivation of this work. The use of thermal energy storage can also help with the peak load shift of power grids[4], creating additional benefits[5].

Some attempts have been made to use PCMs for air conditioning applications. Our recent work on the PCM based air conditioning system showed that, when integrating with the TES, the system efficiency and thermal comfort was improved[6][7]. Said et al.[8] employed the PCM to capture the cold energy from ambient air at night which was then used to cool the air conditioning condenser at daytime. In this way, energy consumption saving was found to achieve up to 8.95%. Allouchal et al. [9] dynamically simulated an air conditioning system with PCM cold storage. They indicated that integrating the PCM based latent heat storage with the air conditioning system lead to a more stable system with higher indoor comfort. Al-Aifan et al. [10]. applied dimethyl adipate with a phase change temperature at around 9.92 °C

to the combined variable refrigerant volume and cool thermal energy storage air conditioning system. It was found that the indoor temperature was maintained at 24 °C for year-round operational conditions. The reduced cooling capacities and reduced combined power consumption contributed to the improved performance of the combined system. The authors concluded that the proposed system would be beneficial to meet indoor comfort cooling without sacrificing energy efficiency. Sun et al. [11] introduced a PCM based air conditioning technique for telecommunications base stations. The simulations combined with the experimental evaluations showed that the adjusted energy efficiency ratio of the new system could be enhanced more than 4 times compared to the normal air conditioner with an estimated energy saving potential at 50%. Chen et al.[12] studied the ventilation systems with thermal energy storage for space cooling in air-conditioned buildings during the summer. The overall electricity energy consumption of the TES system was calculated and compared to a base case without night ventilation and a case with a conventional night ventilation system. It was reported that with changing the indoor temperature setpoint from 24 to 28 °C, the seasonal electric energy saving ratio by using the TES system over the base case increased from 16.9% to 50.8%, while that against the conventional night ventilation system increased from 9.2% to 33.6%.

These studies also indicated the importance of the properties of PCMs for which numerous studies have been carried out. PCMs can be classified broadly into two categories of organic and inorganic materials. Examples of organic PCMs include paraffin wax, high-chain alkane, fatty acids, and fatty acids esters, which are mostly for applications below 180 ^{o}C. Examples of inorganic PCMs include hydrates (mainly for applications at temperatures below <120 ^{o}C), molten salts and metallic materials (for applications at temperatures over 200-1400 ^{o}C). Among these PCMs, paraffin is considered to be among the most suitable PCMs for building

applications due to suitable phase transition temperature range, high latent heat, little supercool[13], being chemically inert[14] and low toxicity [15].

The use of paraffins based PCMs suffers from their low thermal conductivities, which limits charge/discharge rates needed for effective temperature regulation of an air-conditioning system [16][17]. This calls for the development of effective measures to overcome the limitations. As mentioned above, air-conditioning systems often use air as a heat transfer fluid. Air has a very low thermal conductivity and enhancement of air side heat transfer can also be rate limited. Two methods have been proposed to address these issues: one is to use extended surfaces such as fins in both air and PCM sides [18][19]and multi-tubes[20][21]; the other one is to enhance thermal properties of PCMs such as the addition of thermal conductivity enhancer in PCMs[22]. A brief summary of the literature on the effectiveness of the two methods is given in the following.

The use of extended surfaces Tao and He [23] performed a modelling study on the charging behaviour of a PCM based heat exchange unit with fins as extended surface and showed that the use of the fins reduced the discharge time by 71.2%. Sciacovelli et al. [24] employed fins to enhance heat transfer of a shell-and-tube based PCM storage device and found an enhancement of 24% with Y-shaped fins with two bifurcations. Ye et al. [25] numerically studied flow and heat transfer behaviour of a paraffin-based storage device with plate-like fins and observed small pockets of unsolidified PCM and formation of a vortex of air at the top of the PCM bed at the end of heat release process. Stritih [26] experimentally studied a PCM based rectangular heat storage device with a finned surface and showed that the use of the fins reduced the heat release time by 40%. There are also several numerical studies on the effects of key parameters on storage heat exchanger performance; see for example El Qarnia et al. [27], Jmal and Baccar [28] and Yang et al.[29].

The use of thermal conductivity enhancers A number of thermal conductivity enhancers have been studied and shown to be highly effective to increase the thermal conductivity of PCMs. For example, Li et al. [30] added 2.7 wt.% of graphite to a PEG-based PCM and obtained a 100% enhancement in the PCM thermal conductivity. Karaipekli et al. [31] used a small percentage of carbon nanotubes to obtain a considerable extent of thermal conductivity enhancement of an-eicosane based PCM. Atinafu et al. [32] used porous carbons to increase the thermal conductivity of a myristic acid – stearic acid eutectic PCM up to 117.65%. Zou et al. [33] added multi-walled carbon nanotubes and graphene to industrial paraffin wax-based PCM and achieved a thermal conductivity enhancement of up to 124%.

It can be seen that, when integrating the PCM-based TES with the air conditioning systems, the benefits of increasing system efficiency and improving thermal comfort can be achieved. Besides, various studies have been reported on the use of extended surfaces and thermal conductivity enhancers, however, no quantitative comparison has been found, to the best of our knowledge, between the effectiveness of the two methods. This work quantitatively compared the two methods for enhancing the performance of PCM based heat exchange systems through numerical modelling with experimental validation for the first time. First, four configurations were considered: no fins in both the PCM and air sides (no fins); offset strip fins on the airside (air fins); straight fins on the PCM side (PCM fins); and offset strip fins on the airside and straight fins on the PCM side (both fins). PCMs with different thermal conductivities were used to examine the effect of PCM thermal conductivity. Second, the modelling results were used to guide the design and manufacture of a PCM based TES device with offset strip fins on the airside and straight fins on the PCM side (both fins). Besides, our previous work showed that the finned TES device performed the high charging and discharging exergy and energy efficiency[34][35]. Hence, a finned TES device was manufactured, and an experiment rig was constructed using the manufactured TES device.

The charging and discharging behaviour was investigated under different temperatures and velocities of the airside. These experimental results were then used to investigate the working duration, thermal comfort improvement, and air outlet temperature stabilization.

2. Numerical modelling

In this section, the four configurations of the PCM based TES device are described first, followed by boundary and initial conditions. The mathematical model and numerical method are then briefly discussed.

2.1. Physical models

Fig. 1a shows a three-dimensional view of the TES device which consists of PCM chambers and airflow channels. The PCM chambers are rectangular shaped with vertically oriented straight fins; see Fig. 1. Air channels are horizontally arranged with offset strip fins with each 10mm long in the flow direction and orthogonal to the PCM chambers. The air channels and the PCM chambers are periodically arranged and connected with clapboards. The clapboard is the aluminum plates that separate the air and the PCM channel. The use of offset strip fins in the airside was for disturbing airflow to create turbulence for enhancing heat transfer while minimizing pressure drop [36]. The use of straight fins in the PCM side was to minimizing difficulties in the PCM filling process while achieving a required level heat transfer enhancement for the purpose of this study. As the TES device is large, only a small section (marked with red dotted line) was modelling in this study; see Section 2.2 for more details.

2.2. Boundary and initial conditions

In this case, only a single channel with central symmetry in the TES device with a symmetry boundary condition was modelled. The main reasons for the only modelling the small portion are: first, modelling the whole TES device is very time consuming; and second, the geometrical structure of air channels and PCM chambers are symmetrical and periodically

arranged. Fig. 1b shows the detailed geometries of the selected portion for numerical simulation, which has a length of 100mm containing a periodical unit of air channels, PCM chambers, and a clapboard. The height, width and thickness of fins in both air and PCM sides are respectively 9.5 mm, 2.5 mm and 0.2 mm and the offset length of air fins is 10 mm. The width and thickness of the clapboard are 2.5 mm and 0.2 mm, respectively.

The boundary conditions were set on the basis of normal operation of a traditional air conditioning system with air temperature ranging from 284.15 K to 312.15 K and air velocity at 1.20 m/s. During discharging, both the PCM (in solid form) and straight fins were initially set at a temperature of 289.15 K; the inlet air velocity and temperature were given as 1.20 m/s and 312.15 K respectively. During charging, both the PCM (in liquid form) and the straight fins were initially at 298.15 K. The inlet air velocity and temperature were set as 1.20 m/s and 284.15 K, respectively. Tab. 1 gives a summary of these conditions.

2.3. Numerical simulations

The numerical simulations were performed in the ANSYS Fluent. For each of the configurations, the following assumptions were made with rationales also included:

- PCM is uniformed distributed in the PCM chambers and homogeneous in terms of thermos-physical properties – this is justified through carefully PCM filling and degassing processes.
- No heat loss from the modelled parts – this could be achieved by carefully insulating the TES device.
- Negligible effect of natural convection – this is due to densely distributed fins within PCM and little space for PCM to flow [37].

Under the above assumptions, the governing equations for the PCM side include the following mass, momentum, and energy balance equations:

$$\frac{\partial \rho}{\partial t} + \nabla \cdot (\rho \mathbf{v}) = 0 \tag{1}$$

$$\rho \frac{\partial \mathbf{v}}{\partial t} + \rho(\mathbf{v} \cdot \nabla)\mathbf{v} = -\nabla p + \mu \nabla^2 \mathbf{v} \tag{2}$$

$$\frac{\partial}{\partial t}(\rho h) + \nabla \cdot (\rho \mathbf{v} h) = \nabla \cdot (k \nabla T) \tag{3}$$

where v represents the velocity vector; ρ denotes the density; k is the thermal conductivity; h is specific enthalpy and T is temperature. The phase change process was accounted for by using the enthalpy-porosity method, which allows the tracking of the presence of the solid/liquid phase of the PCM by using a parameter called liquid fraction. The specific enthalpy h in Equation (3) is written as:

$$h = h_{ref} + \int_{T_{ref}}^{T} c_p dT + \gamma H \tag{4}$$

where H is the latent heat of fusion of the PCM and liquid fraction γ is defined as:

$$\gamma = \begin{cases} 0 & T \le T_s \\ \dfrac{T - T_s}{T_l - T} & T_s < T < T_l \\ 1 & T \ge T_l \end{cases} \tag{5}$$

where T_s and T_l are respectively the solidification and melting temperature. The air velocity and temperature were obtained by solving the continuity, Navier-Stokes and energy equations, which are similar to Equations (1)-(3) and hence are not repeated here. The Semi-Implicit Method for pressure – Linked Equations (SIMPLE) algorithm was employed for velocity-pressure coupling. The Second Order scheme was used for pressure spatial discretization. Second-order upwind was used for convective terms in momentum and energy equations. The hexahedron mesh strategy was employed in modelling; orthogonal mesh was generated

in PCM and Air domain when the mesh transition was only allowed in the solid domain. As a result, the conformal mesh was formed at the interface of solid and fluid. The dimensionless wall distance y+ was lower than 1, so that the enhanced wall function should be supposed to estimated convective heat transfer. Sensitivity analysis has been done by varying the time step, a time step of 0.1s was chosen to ensure time-step independent results. The convergence was checked with the scaled residuals less than 10^{-6} for the continuity, momentum, and energy equations. In order to satisfy the convergence criteria, the number of iterations for every time step was 50.

3. Experiments and Validation

To validate the numerical model, a pilot-scale experiment was carried out. PCM was filled in a TES device with the same structure as mentioned above. Fins were installed on both of airside and PCM side.

3.1. Phase Change Material

A commercial PCM, RT 18 HC purchased from Rubitherm Technologies GmbH, Germany, was used in the work. A Differential Scanning Calorimeter (DSC-2) from Mettler Toledo was used to determine the thermal properties of the PCM (melting point, latent heat, and specific heat capacity). The measurements used aluminium crucibles containing ~10 mg sample. To obtain reliable and repeatable results, three different samples were measured with each sample measured three times. A sapphire standard was used as a reference to obtain the specific heat capacity. The measurements were done between 0 and 50 °C with a heating/cooling rate of 1 ^{o}C min^{-1} under a nitrogen atmosphere. Table 2 gives a summary of the measurement data. One can see a latent heat of 220 kJ/kg and a melting / freezing temperature range between 17 °C and 19 °C. The specific heat capacities at solid-state (10 °C)

and liquid (30 °C) state were measured to be 1.9 ±0.2 kJ/(kg·K) and 2.0 ±0.2 kJ/(kg·K), respectively.

A laser flash analyzer (LFA427, Netzsch) was used to measure the thermal diffusivity of the PCM with a platinum crucible. The measurements were carried out in an air atmosphere. Tab. 2 shows the results. One can see that the average thermal conductivity of the PCM for both solid and liquid phases is 0.2 W/(m·K).

3.2. Experiment system

Fig. 2 gives a schematic diagram of the experimental set-up, which consists mainly of the TES device as described on Section 2, a commercial air conditioning unit (a fixed-frequency air conditioner unit from Tripp Lite), an airflow and temperature stabilization chamber and a data acquisition unit connected to various sensors. The photo of the experimental test rig is shown in Fig. 3. A Leister Hot air unit was used to provide hot air and the air conditioning unit was from Tripp Lite Company.

The exterior size of the TES device including insulation was 600 mm (length)×300 mm (width)×200 mm (height). Liquid PCM was injected into the TES device through 2mm holes. After PCM in the device became solid, liquid PCM was injected again. The above injections were repeated many times to make sure the device was fulfilled. As a result, a total of 10 kg PCM was filled inside the device. The fins, channels, chambers, and clapboards were made of aluminum. The air chamber has a dimension of 800 mm (height) × 800 mm (width) ×1000 mm (length) to ensure a thorough mixing of cold air from the air conditioner and the hot air from the heater for a precise air temperature control before entering the TES device.

Ten K-type thermocouples were installed in the inlet and outlet of the TES device with 5 in each of the ends. This allowed an average inlet and outlet air temperatures to be obtained from the measurements of the 5 thermocouples. Ten additional K-type thermocouples were

inserted into the interior of the PCM chambers to track the PCM temperature at different positions as a function of time. The locations of the thermocouples inside the PCM are shown in Fig. 4, where the axial distances from the inlet are denoted respectively by T1 and T2 (50mm), T3 and T4 (150mm), T5 and T6 (300mm), T7 and T8 (450mm), and T9 and T10 (550mm). The insertion depth of all the thermocouples is 100 mm.

3.6 Uncertainty analysis

The uncertainty analyses were performed by using a method described by Moffat [38] who derived the following equation for the estimation of the overall uncertainty of measured parameter, δR, as a function of uncertainty of variables, δX_n:

$$\delta R = \sqrt{\sum_{n=1}^{N}\left(\frac{\partial R}{\partial X_n}\right)^2 (\delta X_n)^2} \tag{6}$$

Under the conditions of this study, the maximum uncertainty of the charging and discharging time was estimated at 5.14%.

4. Experimental validation of the modelling results

The mesh independent test for both charge and discharge process was carried out at first, with 351,059, 2,693.220 and 5,362,100 cells for coarse, medium and fine mesh, respectively. The results are shown in Fig. 5a, it could be confirmed that the mesh effect could be neglectable when the mesh is greater than 5,000,000.

Furthermore, since the Reynold number, in this case, could be estimated as lower than 500, which may indicate the flow regime should be laminar. However, the introduction of fins may generate the turbulent flow, so that difference viscous models, including laminar and k-epsilon, and different wall heat transfer model, including standard and enhanced, were also examined. Based on the result in Fig. 5b, it could be confirmed that the k-epsilon turbulent

model with standard wall function model could capture the heat transfer features more accurately.

5. Comparison of TES performances between different fin configurations

Having established confidence in numerical modelling, the TES devices with four fin configurations were simulated. PCMs with different thermal conductivities were also studied for comparison with the use of fins. Based on the modelling results, a TES device was designed and tested. The results are presented and discussed in the following subsections.

5.1 Effects of fin configurations on TES device performance

During charge, the inlet air velocity and temperature were set at respectively 1.2 m/s and 11 ^{o}C (284.15 K). The measured PCM thermal conductivity was used. Fig. 6 shows the simulation results in the form of air temperature and velocity contours with and without fins. As can be seen, the axial air velocity distribution is parabolic in the no fins configuration (Fig. 6d). This indicates a laminar flow regime - consistent with the low Re number (~325) condition. In both fins case, however, the airflow pattern changes significantly, showing regions with increased velocity and flow disturbance (Fig. 6c). Correspondingly, the air temperature increases quickly in both fins case (Fig. 6a) compared to that in the no fins situation (Fig. 6b) due to heat transfer enhancement induced by the airflow disturbance.

Fig. 7 shows the PCM temperature and liquid fraction contours. One can see that the PCM temperature decreases fast in both fins case with (Fig. 7a) than that without fins (Fig. 7b). The solidification starts from regions close to the clapboard in the no fins case (Fig. 7d), whereas it starts in areas close to the clapboard and the fins in the both fins case (Fig. 7c). The liquid fraction of the PCM reduces ~40% in 58 s in the both fins case, while it only reduces by ~10% in 295 s in the no fins configuration. These results clearly demonstrate a

significant heat transfer enhancement by using both fins configuration due to the increased heat transfer area and airflow disturbance.

During discharge, the inlet air velocity and temperature were set at respectively 1.2 m/s and 39 ^{o}C (312.15 K). Fig. 8 and Fig. 9 show the results. Similar to the charging behaviour shown above, more significantly disturbed airflow (Fig. 8d) and faster air temperature reduction (Fig. 8b) can be clearly seen in both fins case than that in the no fins situation (Fig. 8a & Fig. 8c). The PCM starts to melt from areas surrounding the fins and the clapboard in both fins case while the melting process starts only from locations close to the clapboard in the no fins case. The liquid fraction of PCM increases at a much quicker rate in both fins case (Fig. 9c) than that in the no fins configuration.

The liquid fraction data in the charge and discharge processes shown graphically in Figs. 7-9are respectively plotted in Fig. 10a & Fig. 10b as a function of time. One can see that the discharge (melting) process takes ~625s in the no fins case (Fig. 10a); this reduces to 164s for both fins case. The discharge times for the air fin only and PCM only configurations are 180 s and 430 s, respectively. In other words, the discharge time reduces by approximately 74% with both fins, 71% with air fins and 31% with PCM fins, in comparison with the no fins case. These data also clearly demonstrate that the air fins are more effective that the use of PCM fins under the conditions of this study (typically used in air conditioning operations).

Fig. 10b shows the change of liquid fraction during the charge (solidification) process. The total charge time is found to be 1095 s without fins, 168 with both fins, 234 with air fins only and 487 s with PCM fins only. Correspondingly, the charge time reduces by approximately 85% with both fins, 79% with air fins and 56% with PCM fins, in comparison with the no fins case. Clearly, the air fins are more effective than the PCM fins in the charging process. These results are similar to the discharge process discussed above.

5.2 Effects of PCM thermal conductivities

From the discussion above, both the air fins and PCM fins contribute to TES device performance enhancement to a significant extent and the air fins are more effective. A question is raised – can we enhance the PCM side performance by modifying the thermal conductivity of the PCMs? To answer this question, PCMs with different thermal conductivities were examined through modelling and the results were compared with the use of fins. In the modelling, only air fins were used whereas the PCM fins were not used.

Fig. 11 shows the results. One can see that the discharge time decreases with increasing PCM thermal conductivity. When the PCM thermal conductivity increases from 0.2 (the PCM used in experiments in this work) to 1.05 W/(m·K), the discharge time reduces to be comparable to the use of both fins configuration (Fig. 11a). Similarly, for the charging process (Fig. 11b), a PCM with thermal conductivity of ~0.78 W/(m·K) would give the same heat transfer enhancement as the use of the PCM fins. These comparisons indicate that a similar extent of heat transfer performance enhancement can be achieved by either extending the heat transfer area through fins or by using PCMs with high thermal conductivity (~5 times the PCM thermal conductivity used in this work).

The use of fins will result in a slightly higher manufacture cost and limited space drop (~10.8%) for PCM. However, PCMs with desirable phase change temperature and latent heat often do not meet the high thermal conductivity requirement. Currently, the thermal conductivity improvement of PCMs was achieved by using highly thermally conductive additives[39]. This reduces the space for PCM as well, increases the costs and in some cases increases the complexity (e.g. phase separation). The limited cycling life is also a big challenge for the composite PCMs containing thermal conductive particles[40]. Therefore, by the advantages of easy manufacture and lightweight, the use of fins is still a highly effective option.

5.3 Performance of the TES device with both fins

Based on the results presented above, a TES device with both fins was designed and manufactured and integrated with an air conditioning unit; see Section 3.2 for the experimental system. The charge and discharge behaviour of such a system was investigated and the results are presented in the following.

Evolution of PCM temperature during charge and discharge processes the charge and discharge behaviour was studied at different inlet air temperatures with a constant average air velocity of 1.25 m/s. Figs. 12 and 13 show the results respectively during discharge and charge processes. One can see that the temperature profiles at T1, T3, T5, T7, and T9 are almost the same as those respectively at T2, T4, T6, T8, and T10, indicating a rather uniform lateral temperature distribution in the designed TES device. Fig. 12 also shows that the melting front of the PCM (denoted by the sudden temperature increase) moves with time and the front is diffusive due to reasons mentioned earlier. At the inlet air temperatures studied in this work (30 °C and 39 °C), the outlet air temperature is seen to be cooled down to around 18 °C in seconds and such a temperature is kept constant for ~3600 s and 2300 s respectively for the air inlet temperatures of 30 °C and 39 °C.

During charge (Fig. 13), a similar conclusion to the discharge process can be drawn in terms of the lateral temperature distribution uniformity. One can also notice that the motion of the solidification front of the PCM with time as well as the diffusive nature of the solidification front at different axial positions. A comparison between Fig. 13a and Fig. 13b also suggests that a significantly increased charge time would be needed for charges at a high charge temperature; see below for a quantitative comparison.

TES device operating duration For normal operation of an air-conditioning system, the outlet air temperature is expected to be between 16-20 °C. As a result, we take the operating

duration (also termed as a working period) as the period when the TES device has an outlet air temperature between 16-20 °C. In addition, we expect an efficient PCM TES device should maintain the outlet air temperature stabilized around the phase change point and hence we regard the PCM based TES device as optimal if the deviation is within 1^{o}C from the phase change point, namely, between 17 °C and 19 °C in this study, for a long period.

Fig.14 shows the operating duration of the designed TES device. One can see that, with a decrease in the inlet air temperature from 40 °C to 30 °C, the operating duration increases by 58.4%. With the inlet temperature decreases, both the operating duration and the optimal operating duration increase, and the optimal operating duration accounts for 67.3%, 56.0% and 56.1% of the total operating period at inlet air temperatures at 30 °C, 35 °C and 40 °C respectively.

Comparison of air outlet temperature of the system with and without the TES device

Fig.15 compares the air outlet temperature of the air conditioning system with and without the TES device. It can be seen that the system with the TES device provides a smooth outlet air temperature, whereas the air outlet temperature fluctuates significantly between ~0 and ~17 ^{o}C every ~300 s. Such a highly frequent and high amplitude fluctuation would imply a more frequent start-stop of the compressor of the fixed-frequency air conditioner, leading to higher energy consumption. This also clearly demonstrates that the TES based air-conditioning system gives a significantly improved thermal comfort, and potentially lower energy consumption. Besides, the system work reported by us recently showed that the system efficiency could be improved with increased thermal comfort, which was caused by the reduction of the ON-OFF times of the compressor [6][7].

6. Conclusions

The work presented in this paper concerns the performance enhancement of a PCM based TES device for air-conditioning applications. The particular focus is on enhancing heat transfer by extending heat transfer surfaces (fins) in both the PCM and air sides and adding heat transfer enhancement materials in the PCM. First, TES devices of four different configurations were modelled and compared. The modelling results were then validated by experimental data. The results indicated a significant extent of performance enhancement of the TES device due to the use of fins. The airside fins were found to be more effective than the PCM side fins. The discharging and charging time reduced by approximately 74% and 85% with both fins in comparison with the no fin case, respectively.

The results also showed that the heat transfer enhancement due to the PCM side fins could be achieved by increasing PCM thermal conductivity. When the PCM thermal conductivity increased from 0.2 to 1.05 W/(m·K) and 0.78 W/(m·K), the discharging and charging time reduced to be comparable to the use of both fins configuration.

However, improving the thermal conductivity of the PCMs caused the increase in the costs and in some cases increased the complexity (e.g. phase separation). Therefore, a PCM-based TES device was designed and manufactured based on the above results. The device was integrated into an air-conditioning system and experimentally tested. The results showed that, for both charge and discharge processes, the system level performance was significantly improved, leading to an increased extent of thermal comfort and decreased outlet temperature fluctuations. The obtained results can contribute to the design and optimization of the TES device for an air conditioning application.

Acknowledgments

The authors would like to acknowledge partial financial support from EPSRC under EP/P004709/1, EP/P003435/1 and EP/P003605/1.

References

[1] González-Gil A, Palacin R, Batty P, Powell JP. A systems approach to reduce urban rail energy consumption. Energy Convers Manag 2014;80:509–24. doi:10.1016/j.enconman.2014.01.060.

[2] She X, Cong L, Nie B, Leng G, Peng H, Chen Y, et al. Energy-efficient and -economic technologies for air conditioning with vapor compression refrigeration: A comprehensive review. Appl Energy 2018;232:157–86. doi:10.1016/j.apenergy.2018.09.067.

[3] Spagnuolo A, Petraglia A, Vetromile C, Formosi R, Lubritto C. Monitoring and optimization of energy consumption of base transceiver stations. Energy 2015;81:286–93. doi:10.1016/j.energy.2014.12.040.

[4] Hirmiz R, Teamah HM, Lightstone MF, Cotton JS. Performance of heat pump integrated phase change material thermal storage for electric load shifting in building demand side management. Energy Build 2019;190:103–18. doi:10.1016/j.enbuild.2019.02.026.

[5] Saffari M, de Gracia A, Fernández C, Belusko M, Boer D, Cabeza LF. Optimized demand side management (DSM) of peak electricity demand by coupling low temperature thermal energy storage (TES) and solar PV. Appl Energy 2018;211:604–16. doi:10.1016/j.apenergy.2017.11.063.

[6] Nie B, She X, Du Z, Xie C, Li Y, He Z, et al. System performance and economic assessment of a thermal energy storage based air-conditioning unit for transport applications. Appl Energy 2019;251:113254. doi:10.1016/j.apenergy.2019.05.057.

[7] Nie B, She X, Yu Q, Zou B, Zhao Y, Li Y, et al. Experimental study of charging a compact PCM energy storage device for transport application with dynamic exergy

analysis. Energy Convers Manag 2019;196:536–44. doi:10.1016/j.enconman.2019.06.032.

[8] Said MA, HASSAN H. A study on the Thermal Energy Storage of Different Phase Change Materials incorporated with the Condenser of Air-Conditioning Unit and their Effect on the Unit Performance. Energy Build 2019;202:109353. doi:10.1016/j.enbuild.2019.109353.

[9] Allouche Y, Varga S, Bouden C, Oliveira AC. Dynamic simulation of an integrated solar-driven ejector based air conditioning system with PCM cold storage. Appl Energy 2017;190:600–11. doi:10.1016/j.apenergy.2017.01.001.

[10] Al-Aifan B, Parameshwaran R, Mehta K, Karunakaran R. Évaluation De La Performance D'Un Volume De Frigorigène Variable Combiné À Un Système De Stockage D'Énergie Thermique Froide Pour Des Applications De Conditionnement D'Air. Int J Refrig 2017;76:271–95. doi:10.1016/j.ijrefrig.2017.02.008.

[11] Sun X, Zhang Q, Medina MA, Liu Y, Liao S. A study on the use of phase change materials (PCMs) in combination with a natural cold source for space cooling in telecommunications base stations (TBSs) in China. Appl Energy 2014;117:95–103. doi:10.1016/j.apenergy.2013.12.010.

[12] Chen X, Zhang Q, John Z, Ma X. Potential of ventilation systems with thermal energy storage using PCMs applied to air conditioned buildings. Renew Energy 2019;138:39–53. doi:10.1016/j.renene.2019.01.026.

[13] Li M, Guo Q, Nutt S. Carbon nanotube/paraffin/montmorillonite composite phase change material for thermal energy storage. Sol Energy 2017;146:1–7. doi:10.1016/j.solener.2017.02.003.

[14] Li G, Hwang Y, Radermacher R. Review of cold storage materials for air conditioning

application. Int J Refrig 2012;35:2053–77. doi:10.1016/j.ijrefrig.2012.06.003.

[15] Belessiotis G V, Papadokostaki KG, Favvas EP. Preparation and investigation of distinct and shape stable para ffi n / SiO 2 composite PCM nanospheres 2018;168:382–94. doi:10.1016/j.enconman.2018.04.059.

[16] Fan L, Khodadadi JM. Thermal conductivity enhancement of phase change materials for thermal energy storage: A review. Renew Sustain Energy Rev 2011;15:24–46. doi:10.1016/j.rser.2010.08.007.

[17] Liu L, Su D, Tang Y, Fang G. Thermal conductivity enhancement of phase change materials for thermal energy storage: A review. Renew Sustain Energy Rev 2016;62:305–17. doi:10.1016/j.rser.2016.04.057.

[18] Medrano M, Yilmaz MO, Nogués M, Martorell I, Roca J, Cabeza LF. Experimental evaluation of commercial heat exchangers for use as PCM thermal storage systems. Appl Energy 2009;86:2047–55. doi:10.1016/j.apenergy.2009.01.014.

[19] Al-Abidi AA, Mat S, Sopian K, Sulaiman MY, Mohammad AT. Experimental study of melting and solidification of PCM in a triplex tube heat exchanger with fins. Energy Build 2014;68:33–41. doi:10.1016/j.enbuild.2013.09.007.

[20] Esapour M, Hamzehnezhad A, Rabienataj Darzi AA, Jourabian M. Melting and solidification of PCM embedded in porous metal foam in horizontal multi-tube heat storage system. Energy Convers Manag 2018;171:398–410. doi:10.1016/j.enconman.2018.05.086.

[21] Esapour M, Hosseini MJ, Ranjbar AA, Pahamli Y, Bahrampoury R. Phase change in multi-tube heat exchangers. Renew Energy 2016;85:1017–25. doi:10.1016/j.renene.2015.07.063.

[22] Mahdi JM, Nsofor EC. Solidi fi cation enhancement of PCM in a triplex-tube thermal

energy storage system with nanoparticles and fi ns. Appl Energy 2018;211:975–86. doi:10.1016/j.apenergy.2017.11.082.

[23] Tao YB, He YL. Numerical study on performance enhancement of shell-and-tube latent heat storage unit. Int Commun Heat Mass Transf 2015;67:147–52. doi:10.1016/j.icheatmasstransfer.2015.07.013.

[24] Sciacovelli A, Gagliardi F, Verda V. Maximization of performance of a PCM latent heat storage system with innovative fins. Appl Energy 2015;137:707–15. doi:10.1016/j.apenergy.2014.07.015.

[25] Ye WB, Zhu DS, Wang N. Numerical simulation on phase-change thermal storage/release in a plate-fin unit. Appl Therm Eng 2011;31:3871–84. doi:10.1016/j.applthermaleng.2011.07.035.

[26] Stritih U. An experimental study of enhanced heat transfer in rectangular PCM thermal storage. Int J Heat Mass Transf 2004;47:2841–7. doi:10.1016/j.ijheatmasstransfer.2004.02.001.

[27] El Qarnia H, Draoui A, Lakhal EK. Computation of melting with natural convection inside a rectangular enclosure heated by discrete protruding heat sources. Appl Math Model 2013;37:3968–81. doi:10.1016/j.apm.2012.08.021.

[28] Jmal I, Baccar M. Numerical study of PCM solidification in a finned tube thermal storage including natural convection. Appl Therm Eng 2015;84:320–30. doi:10.1016/j.applthermaleng.2015.03.065.

[29] Yang L, Peng H, Ling X, Dong H. Numerical analysis on performance of naphthalene phase change thermal storage system in aluminum plate-fin unit. Heat Mass Transf Und Stoffuebertragung 2014;51:195–207. doi:10.1007/s00231-014-1400-7.

[30] Li J, He L, Liu T, Cao X, Zhu H. Preparation and characterization of PEG/SiO2

composites as shape-stabilized phase change materials for thermal energy storage. Sol Energy Mater Sol Cells 2013;118:48–53. doi:10.1016/j.solmat.2013.07.017.

[31] Karaipekli A, Biçer A, Sarı A, Tyagi VV. Thermal characteristics of expanded perlite/paraffin composite phase change material with enhanced thermal conductivity using carbon nanotubes. Energy Convers Manag 2017;134:373–81. doi:10.1016/j.enconman.2016.12.053.

[32] Atinafu DG, Dong W, Huang X, Gao H, Wang G. Introduction of organic-organic eutectic PCM in mesoporous N-doped carbons for enhanced thermal conductivity and energy storage capacity. Appl Energy 2018;211:1203–15. doi:10.1016/j.apenergy.2017.12.025.

[33] Zou D, Ma X, Liu X, Zheng P, Hu Y. Thermal performance enhancement of composite phase change materials (PCM) using graphene and carbon nanotubes as additives for the potential application in lithium-ion power battery. Int J Heat Mass Transf 2018;120:33–41. doi:10.1016/j.ijheatmasstransfer.2017.12.024.

[34] Nie B, She X, Zou B, Li Y, Li Y, Ding Y. Discharging performance enhancement of a phase change material based thermal energy storage device for transport air-conditioning applications. Appl Therm Eng 2020;165:114582. doi:10.1016/j.applthermaleng.2019.114582.

[35] Nie B, She X, Yu Q, Zou B, Zhao Y, Li Y, et al. Experimental study of charging a compact PCM energy storage device for transport application with dynamic exergy analysis. Energy Convers Manag 2019;196:536–44. doi:10.1016/j.enconman.2019.06.032.

[36] Peng H, Ling X, Li J. Performance investigation of an innovative offset strip fin arrays in compact heat exchangers. Energy Convers Manag 2014;80:287–97.

doi:10.1016/j.enconman.2014.01.050.

[37] Bertrand O, Binet B, Combeau H, Couturier S, Delannoy Y, Gobin D, et al. Melting driven by natural convection A comparison exercise: first results. Int J Therm Sci 1999;38:5–26. doi:10.1016/S0035-3159(99)80013-0.

[38] Moffat RJ. Describing the uncertainties in experimental results. Exp Therm Fluid Sci 1988;1:3–17. doi:10.1016/0894-1777(88)90043-X.

[39] Lin Y, Jia Y, Alva G, Fang G. Review on thermal conductivity enhancement, thermal properties and applications of phase change materials in thermal energy storage. Renew Sustain Energy Rev 2018;82:2730–42. doi:10.1016/j.rser.2017.10.002.

[40] Cabeza LF, Castell A, Barreneche C, De Gracia A, Fernández AI. Materials used as PCM in thermal energy storage in buildings: A review. Renew Sustain Energy Rev 2011;15:1675–95. doi:10.1016/j.rser.2010.11.018.

Figs:

Fig.1 The TES device for modelling and experimental validation.

Fig. 2 Schematic diagram of the experimental rig for the TES device measurements

Fig. 3 Photo of the experimental rig for the TES device measurements

Fig. 4 Thermocouple positions inside the TES device (*mm*)

Fig. 5 Grid independency and model selection

Fig.6 Contours of the charging process: Air temperature for the both fins configuration (a) and the no fins configuration (b); Air velocity for the both fins configuration(c) and the no fins configuration (d).

Fig. 7 Contours during charging process: PCM temperature for the both fins case (a) and the no fins case (b); PCM liquid fraction for the both fins scenario(c) and the no fins case (d).

Fig .8 Contours during discharge: Air temperature for the no fins case (a) and the both fins case (b); Air velocity for the no fins case (c) and the both fins case(d).

Fig. 9 Contours during discharge: PCM temperature for the both fins case(a) and the no fins case(b); PCM liquid fraction for the both fins case(c) and the no fins case(d).

Fig. 10 Time evolution of the liquid fraction during the discharge (a) and charge (b) processes with various configurations.

Fig. 11 Discharge time (a) and charge time for PCM with different thermal conductivities

Fig. 12 Evolution of axial temperature of air and PCM during discharge with air inlet temperature of 30°C (a) and 39°C (b)

Fig. 13 Evolution of axial temperature of air and PCM during charge with an inlet air temperature of 11°C (a) and 15°C (b)

Fig. 14 Operating duration for the designed TES device at inlet air velocity of 1.25m/s

Fig. 15 Comparison of the air outlet temperature of the system with and without the TES device

Tabs:

Tab. 1 Initial conditions for modelling the charging and discharging processes

Tab. 2 Thermophysical properties of RT18 HC PCM

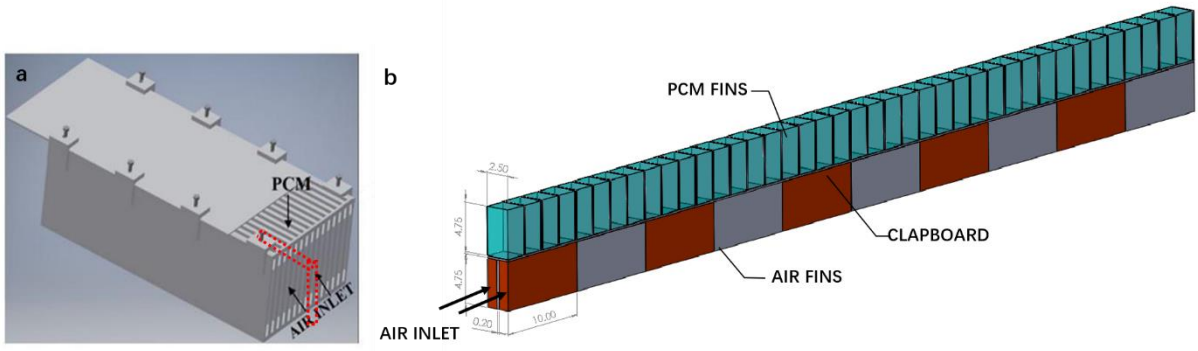

Fig.1 The TES device for modelling and experimental validation.

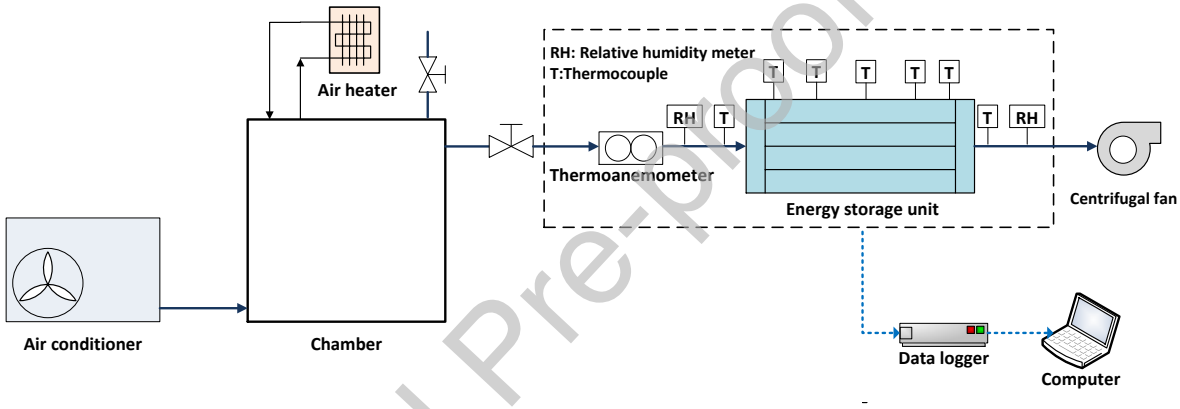

Fig. 2 Schematic diagram of the experimental rig for the TES device measurements

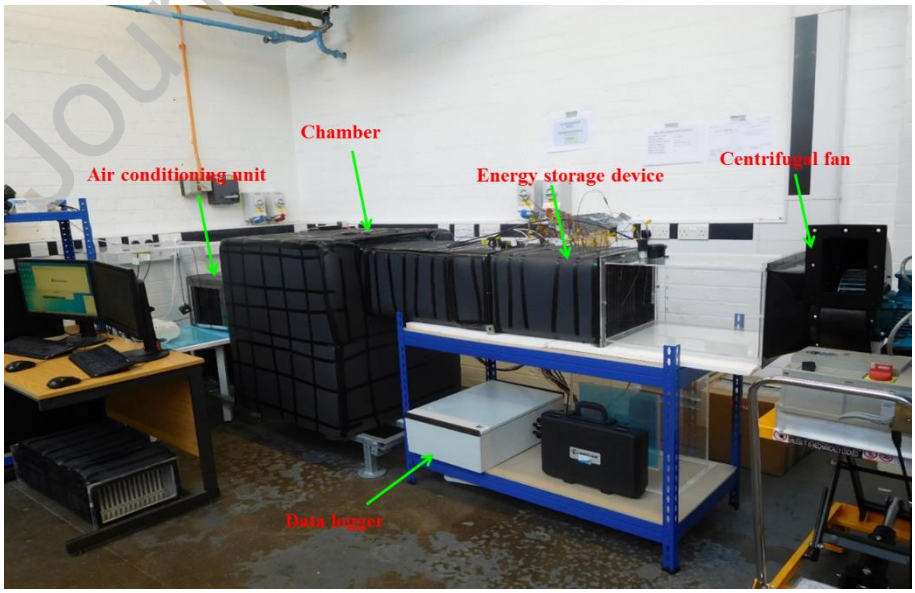

Fig. 3 Photo of the experimental rig for the TES device measurements

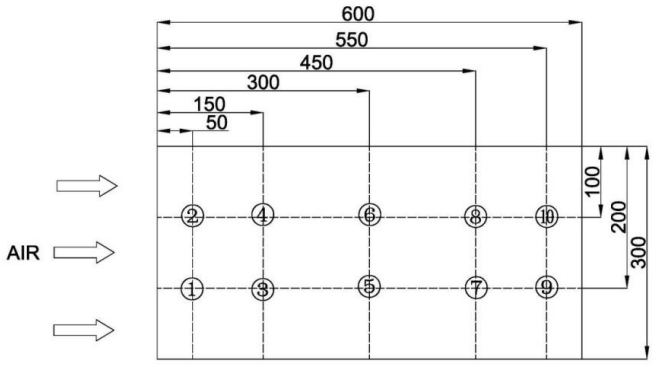

Fig. 4 Thermocouple positions inside the TES device (*mm*)

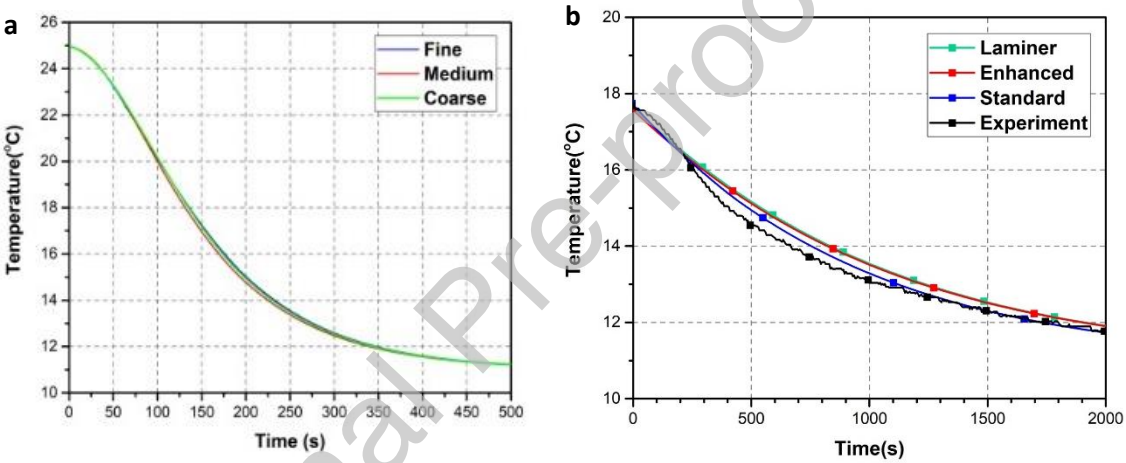

Fig. 5 Grid independency and model selection

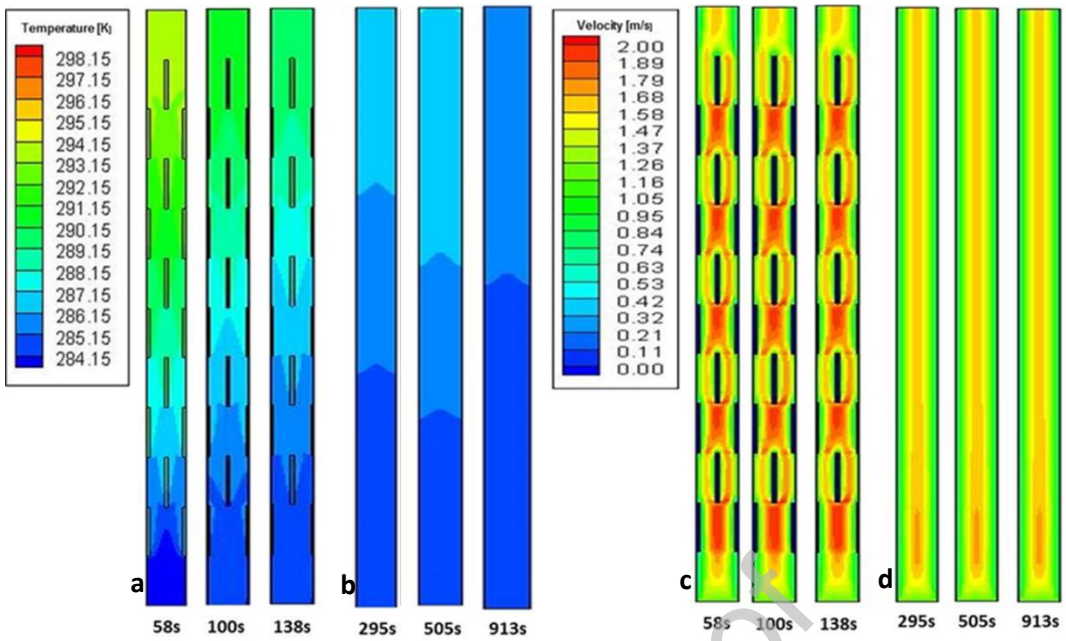

Fig. 6 Contours of the charging process: Air temperature for the both fins configuration (a) and the no fins configuration (b); Air velocity for the both fins configuration(c) and the no fins configuration (d).

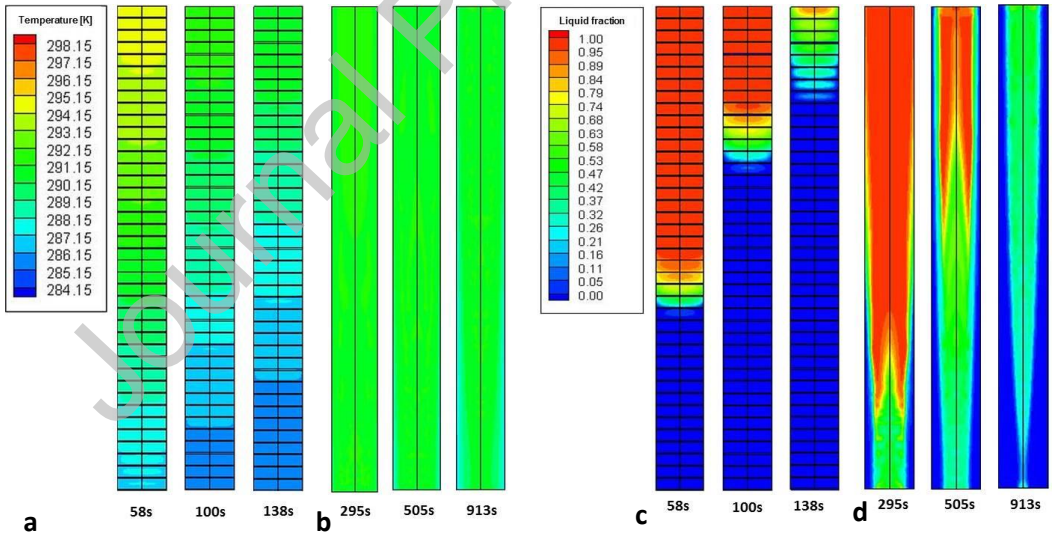

Fig. 7 Contours during charging process: PCM temperature for the both fins case (a) and the no fins case (b); PCM liquid fraction for the both fins scenario(c) and the no fins case (d).

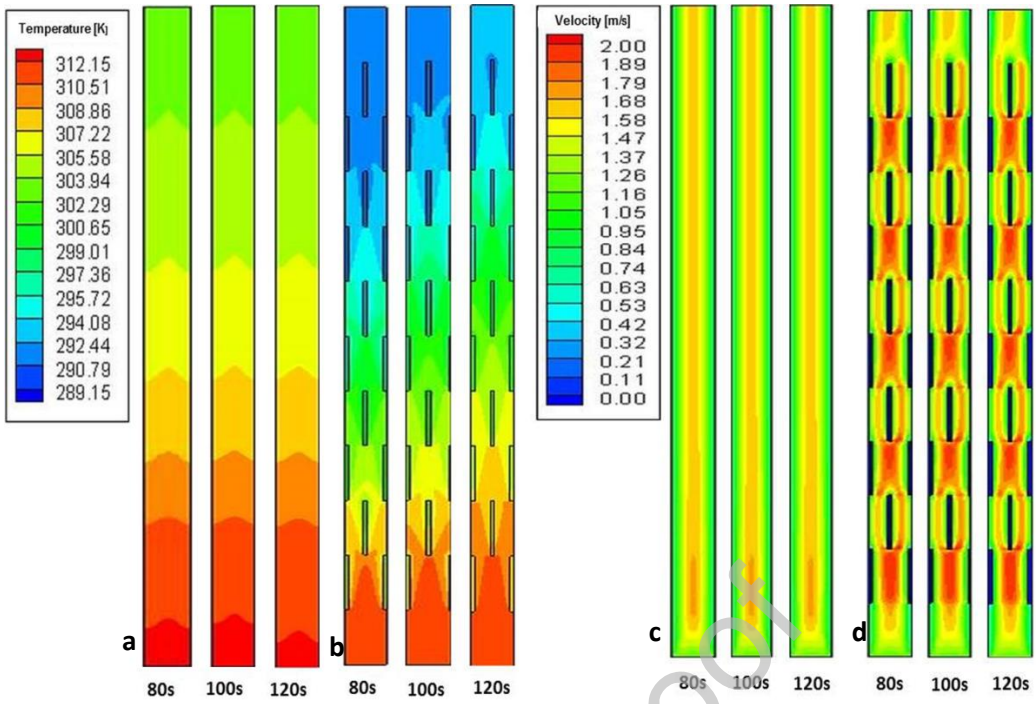

Fig. 8 Contours during discharge: Air temperature for the no fins case (a) and the both fins case (b); Air velocity for the no fins case (c) and the both fins case(d).

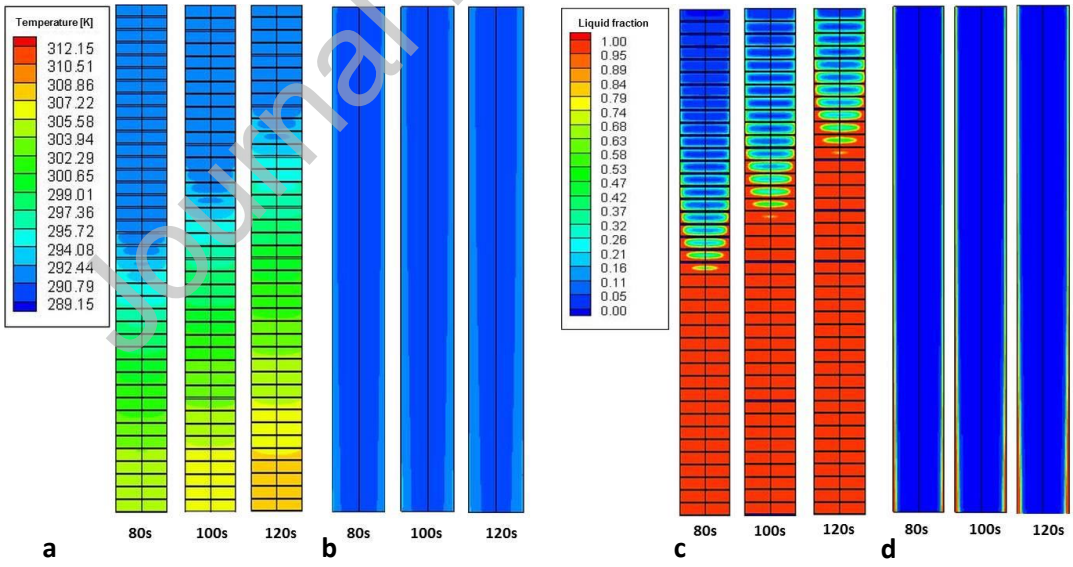

Fig. 9 Contours during discharge: PCM temperature for the both fins case(a) and the no fins case(b); PCM liquid fraction for the both fins case(c) and the no fins case(d).

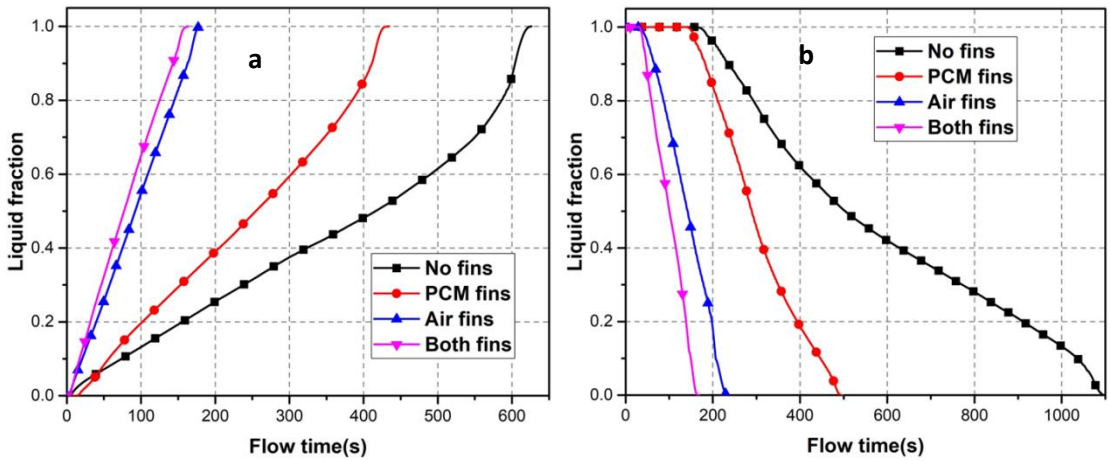

Fig. 10 Time evolution of the liquid fraction during the discharge (a) and charge (b) processes with various configurations.

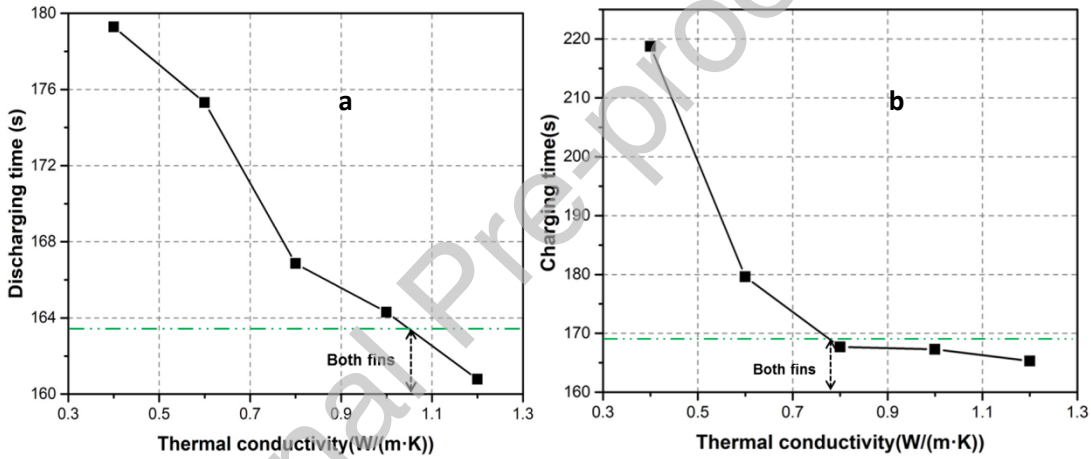

Fig. 11 Discharge time (a) and charge time for PCM with different thermal conductivities

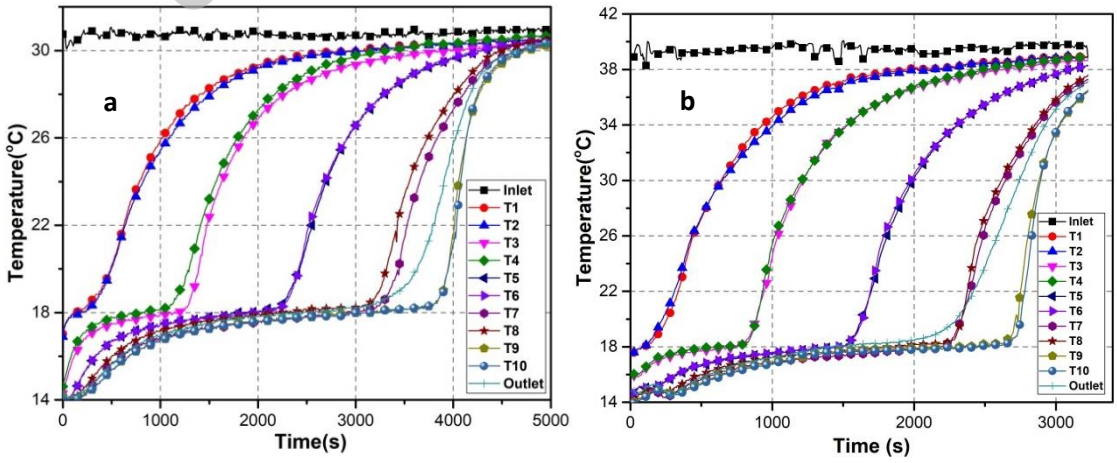

Fig. 12 Evolution of axial temperature of air and PCM during discharge with air inlet temperature of 30°C (a) and 39°C (b).

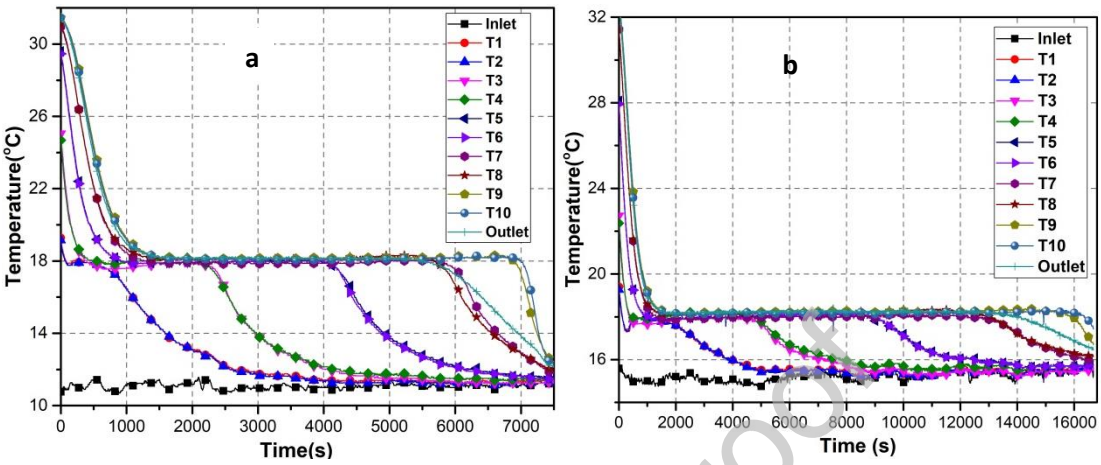

Fig. 13 Evolution of axial temperature of air and PCM during charge with an inlet air temperature of 11°C (a) and 15°C (b)

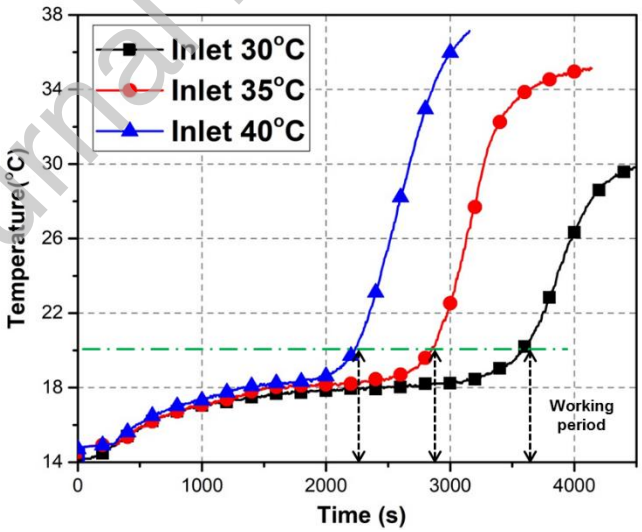

Fig. 14 Operating duration for the designed TES device at inlet air velocity of 1.25m/s

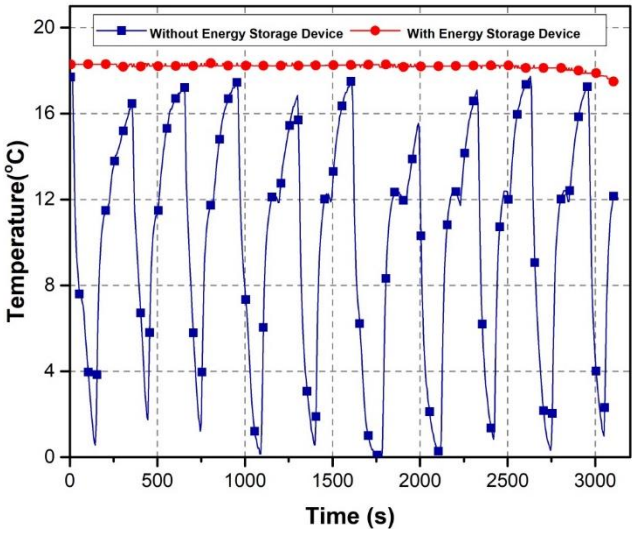

Fig. 15 Comparison of the air outlet temperature of the system with and without the TES device

Tab. 1 Initial conditions for modelling the charging and discharging processes

Parameters	Charging	Discharging
Inlet air temperature (K)	284.15	312.15
Inlet air velocity (m/s)	1.20	1.20
Initial PCM phase temperature (K)	Liquid, 298.15	Solid, 289.15
Initial air fin and clapboard temperature (K)	298.15	289.15
Initial PCM side fin temperature (K)	298.15	289.15

Tab. 2 Thermophysical properties of RT18 HC PCM

Density kg/m^3	Latent heat kJ/kg	Melting temperature °C	Freezing temperature °C	Specific heat capacity kJ/(kg·K)	Thermal conductivity W/(m·K)
880(s); 770(l)	220	17-19 (18)	19 -17 (18)	1.9 ±0.2 (s); 2.0 ±0.2 (l)	0.2

GRAPHICAL ABSTRACT

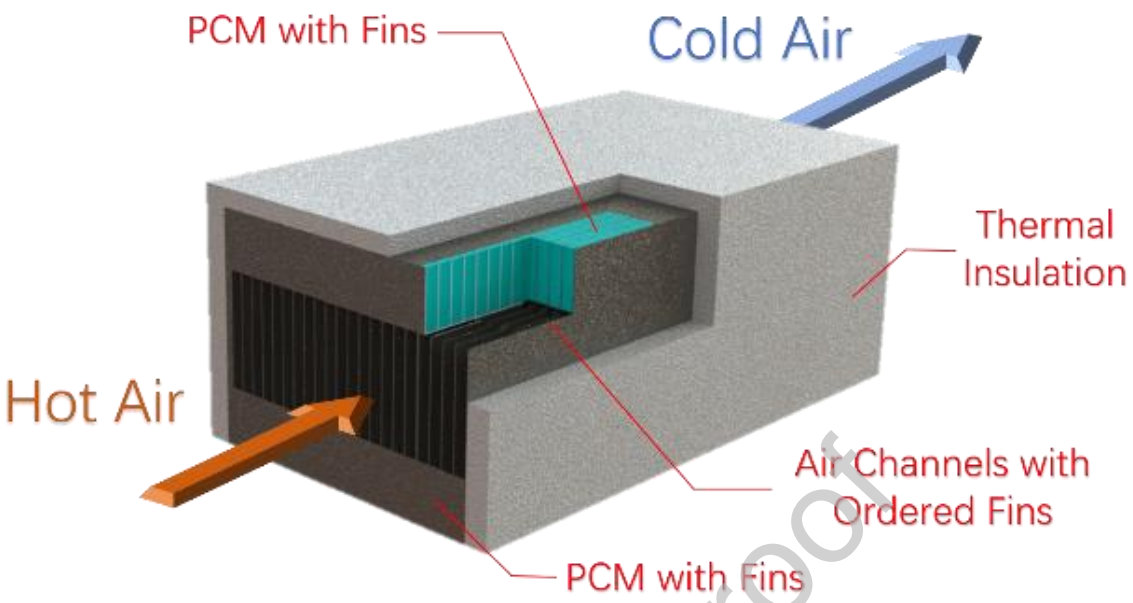

Statement

The contributions from the authors are as follows:

Binjian Nie: Modelling and experimental investigation, Data Curation, Writing - Original Draft;

Zheng Du: Modelling work;

Boyang Zou: Writing- Reviewing and Editing;

Yongliang Li: Supervision, modelling;

Yulong Ding: Supervision, Conceptualization.

Declaration of interests

☒ The authors declare that they have no known competing financial interests or personal relationships that could have appeared to influence the work reported in this paper.

☐The authors declare the following financial interests/personal relationships which may be considered as potential competing interests: